Excitation of positive-parity states in electron scattering from ^{90}Zr

J. Heisenberg, J. Dawson, T. Milliman, and O. Schwentker*

University of New Hampshire, Durham, New Hampshire 03824

J. Lichtenstadt

Tel-Aviv University, Ramat Aviv, Tel-Aviv, Israel 69978

C. N. Papanicolas

University of Illinois, Urbana, Illinois 61801

J. Wise and J. S. McCarthy

University of Virginia, Charlottesville, Virginia 22901

N. Hintz

University of Minnesota, Minneapolis, Minnesota 55455

H. P. Blok

Vrije Universiteit, Amsterdam, The Netherlands

(Received 5 July 1983)

Electron scattering cross sections for ^{90}Zr have been measured with a resolution of less than 40 keV in a momentum transfer range between $0.4 < q < 3.1$ fm^{-1} both at forward angles and at 160°, which allows a separation of longitudinal and transverse form factors. The analysis of the positive-parity states (including previous data for some of the states) results in transition densities. Most densities are compared to various model calculations. The density of the 8^+ level is used to determine the radius of the $g_{9/2}$ proton orbit as $R(g_{9/2}) = 5.035 \pm 0.045$ fm.

I. INTRODUCTION

In recent years, with the advent of new accelerators, electron scattering has been recognized as a very powerful tool in the study of nuclear levels. The advantage of the electron as compared to other probes for nuclei lies in the precision of the probe for the determination of the nuclear densities. This precision originates from the well-known properties of the electromagnetic interaction on the one hand, and from the weakness of the probe on the other hand, which allows us to treat the scattering process in the distorted-wave Born approximation.

As a consequence, the questions posed by electron scattering results differ from other probes. While most of the present concepts in nuclear physics have been developed in concurrence with results from other probes, the new electron scattering results stress the quantitative aspect of the ability to master the many body system. For that reason, precise results are particulary interesting in those regions of the periodic system where theories are most applicable, i.e., around the closed shell nuclei.

We present in this paper results from an electron scattering experiment on ^{90}Zr for positive-parity levels below about 5 MeV in excitation energy. In this region, with the resolution obtained, the level density still allows a fairly clean separation of most of the levels so that we can make an unambiguous interpretation of our data.

The neutron number $N = 50$ provides a good shell clo-

sure for the neutrons with all orbits up to the $1g_{9/2}$ orbit filled. With $Z = 40$, the protons should fill the orbits up to the $2p_{1/2}$ orbit, which would prohibit any $0\hbar\omega$ positive-parity transitions. In that case, the low-lying spectrum should be dominated by the negative parity transitions of protons from the $2p$ or $1f$ orbit to the $1g_{9/2}$ orbit. However, it is generally known that the proton shell closure is not as good, and that substantial configuration mixing occurs in the ground state of ^{90}Zr, resulting in a considerable occupation probability for the $1g_{9/2}$ orbit.[1] This then leads to $0\hbar\omega$ transitions that arise from the recoupling of the pairs in the $1g_{9/2}$ orbit or from the ^{88}Sr core excitations which are also observed.[2] The first states dominated by individual neutron ph components corresponding to the transition from the $1g_{9/2}$ orbit to the $2d_{5/2}$ orbit appear between 4.2–5.1 MeV.[3,4]

When comparing the experimental results with those calculated from nuclear models, e.g., the shell model, two points are of prime importance: the degree in which pairing correlations in the nuclear ground state are taken into account and the size of the configuration space, i.e., the number of ph transitions that are incorporated. The limitations on the last point introduce the need for core polarization corrections. Both aspects can be well studied through electron scattering by comparing the transition densities extracted from the measured cross sections with densities calculated from nuclear models. Pairing correlations will make themselves visible through a renormaliza-

tion of the transition densities calculated within the model space. This renormalization is different for the charge and the current densities. Core polarization will show up as a difference in shape and/or magnitude between the measured and calculated transition densities.

Core polarization is especially important for low-lying collective levels of low multipolarity, as demonstrated by the need to use effective charges when comparing, for instance, measured and calculated $B(E2)$ values. On the other hand, it has been observed in the Pb region that for high-spin electric transitions very little polarization charge is needed,[5,6] so that one can expect fair agreement for high-spin states. It is that aspect that makes the investigation of the large angular-momentum states particularly interesting.

From the many levels observed at excitation energies less than about 5 MeV, we discuss here the positive parity states only. The negative parity states will be presented in a future paper. Low-spin excitations of various kinds as well as several high-spin states occur in this region, allowing a sensitive test of the predictions of nuclear models, especially with respect to questions of core polarization. The experimental details are given in Sec. II. Wherever possible, we have extracted from the data the transition charge densities as described in Sec. III. The best fit parameters for the densities extracted can be found in the Appendix. The results for the various states observed are presented and discussed in Sec. IV. In Sec. V, we compare the measured densities with the results obtained from several nuclear model calculations. This includes a discussion of the apparent need to include core polarization. Section VI contains the discussion about the radial size of the proton $1g_{9/2}$ orbit.

II. EXPERIMENTAL PROCEDURE

The experiment was performed at the MIT-Bates Linear Electron Accelerator using the high-resolution spectrometer facility. This facility has been described elsewhere.[7] Here we report only the features that are relevant to this particular experiment.

Spectra of scattered electrons have been measured in forward direction at scattering angles between 40° and 110° with incident energies between 100 and 368 MeV, and at a scattering angle of 160° with incident energies between 70 and 235 MeV. The forward scattering data cover a momentum transfer range of $0.4 < q < 3.1$ fm^{-1}. This range extends to above twice the Fermi momentum, so transition charge densities can be determined without substantial uncertainties from the unmeasured high momentum-transfer region. At backward angles, a momentum transfer range of $0.7 < q < 2.4$ fm^{-1} has been covered. The targets used were 96.5% enriched ^{90}Zr metallic foils of about 12 mg/cm^2 thickness. For the forward scattering runs at higher energy, two target foils were used together in the transmission mode to give a normal target thickness of 25 mg/cm^2. The typical resolution for these runs was 30—40 keV. In backward direction only a single foil was used in the reflection mode resulting in a resolution of better than 40 keV. Some of the low momentum transfer runs in forward direction were
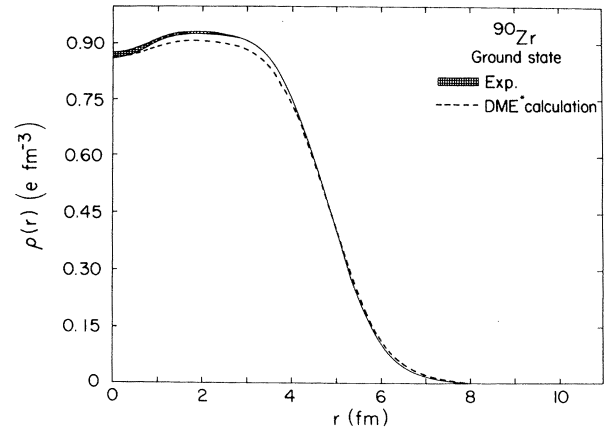

FIG. 1. Ground state charge distribution of ^{90}Zr. The dashed line gives prediction using DME-HF single particle wave functions with partial occupations taken from shell model calculations.

done with single foils in the transmission mode in which a resolution of about 15 keV was obtained.

Since our data at 368 MeV allow us to reduce the incompleteness error in the ground-state charge distribution, we have refitted all available previous data on ^{90}Zr together with our 368 MeV data. These include the data from Fajardo *et al.*,[8] Rothhaas,[9] Phan *et al.*,[10] and Singhal *et al.*[11] In addition, the muonic x-ray data of Fricke *et al.*[12] were used. The data were fitted using the Fourier-Bessel analysis according to Friar and Negele.[13] The resulting charge distribution is shown in Fig. 1 and its resulting Fourier-Bessel parameters are given in Table I.

Generally the inelastic cross sections were measured relative to the elastic cross sections which were calculated with a phase shift code from our fitted ground state charge distribution. Exceptions are the 160° data above 185 MeV where the elastic cross sections were too small to provide a reasonable normalization, and the 368 MeV data that extended beyond the range of the previously existing elastic data. The 160° data above 185 MeV were converted to absolute cross sections taking the nominal values for the target thickness, solid angle, etc., that were shown at lower energies to provide the proper normalization to within 5%. The 368 MeV data were normalized at 40°, where the elastic form factor is still well established. The uncertainty in this normalization was estimated to be 3%, which is due mostly to the uncertainty in incident energy or in efficiency fluctuations across the detector.

TABLE I. Parameters for the ground state charge distribution of ^{90}Zr given as $\rho = \sum A_n j_0(n\pi r/R)$ with $R = 10$ fm.

n	A_n	n	A_n
1	0.046184	7	-0.000079
2	0.030895	8	-0.000758
3	-0.004105	9	0.000134
4	-0.009228	10	0.000038
5	0.000503	11	-0.000015
6	0.002539	12	0.000005

For that reason we have added 3% errors in quadrature to all measured inelastic cross sections.

Effects from channel to channel efficiencies have been reduced by moving the detector several times during the run so that each level samples the efficiency of many channels. The smooth variation in detector efficiency has been measured for several runs by moving the peaks observed in the scattering from BeO across the detector by changing the spectrometer's magnetic field. Using the well-known excitation energies of states in ^{16}O and ^{9}Be, this procedure allowed at the same time to calibrate the dispersion of the spectrometer, the incident energy (through the recoil difference), and the relative efficiencies. In order to correct for the spectrometer's nonlinearities in the dispersion, the data were resorted into equal-width energy bins. At the same time, the data were corrected for relative efficiencies and dead time effects. The cross sections were extracted using a line shape fitting procedure. The line shape was described as the theoretical shape representing the energy distribution after scattering of a monoenergetic beam, folded with a Gaussian shape, representing the experimental resolution. The theoretical shape accounts for radiative effects such as emission of Schwinger radiation, bremsstrahlung, and Landau strag-

gling. A fitted spectrum is shown in Fig. 2.

Figure 2 also shows the level spectrum. The lines indicate levels listed in the Nuclear Data Tables[14] or shown in the high resolution work of van der Bijl et al.[15] Below an excitation energy of 4.2 MeV, the levels of ^{90}Zr are generally well established in energy, spin, and parity. These levels were well resolved in our experiment. The 0^+ level at 1.761 MeV and the 0^+ level at 4.12 MeV are observed only in very few spectra. Generally its cross section was too small. In the region from 4.2 to 5.5 MeV the level density is so large that many levels are not fully resolved. Nevertheless, our experiment allows us to establish several levels not known so far.

III. ANALYSIS AND EXTRACTION OF DENSITIES

The analysis of the differential cross sections has to be done in the distorted-wave Born approximation (DWBA) as the distortion of the electron waves in the Coulomb field of the nucleus is important. Since the physical ideas are more transparent in the plane-wave Born approximation (PWBA) we present that formalism. In PWBA, the cross section is given as

$$\frac{d\sigma}{d\Omega} = 4\pi \left[\frac{d\sigma}{d\Omega}\right]_{\text{Mott}} \eta \left\{ \sum_{\lambda \geq 0} |F_\lambda^C(q)|^2 + \left[\frac{1}{2} + \tan^2\frac{\theta}{2}\right] \sum_{\lambda \geq 1} [\,|F_\lambda^E(q)^2 + |F_\lambda^M(q)|^2]\right\} . \tag{1}$$

Here the Mott cross section is

$$\left[\frac{d\sigma}{d\Omega}\right]_{\text{Mott}} = \left[\frac{\alpha \hbar c \cos\frac{\theta}{2}}{2E_i \sin^2\frac{\theta}{2}}\right]^2 , \tag{2}$$

and the recoil factor η is given through the incident energy E_i, and the target mass M_T as

$$\eta = \left[1 + \frac{2E_i}{M_T c^2}\sin^2\frac{\theta}{2}\right]^{-1} . \tag{3}$$

The form factors F_λ^C, F_λ^E, and F_λ^M containing all the nuclear structure information depend only on the momentum transfer q
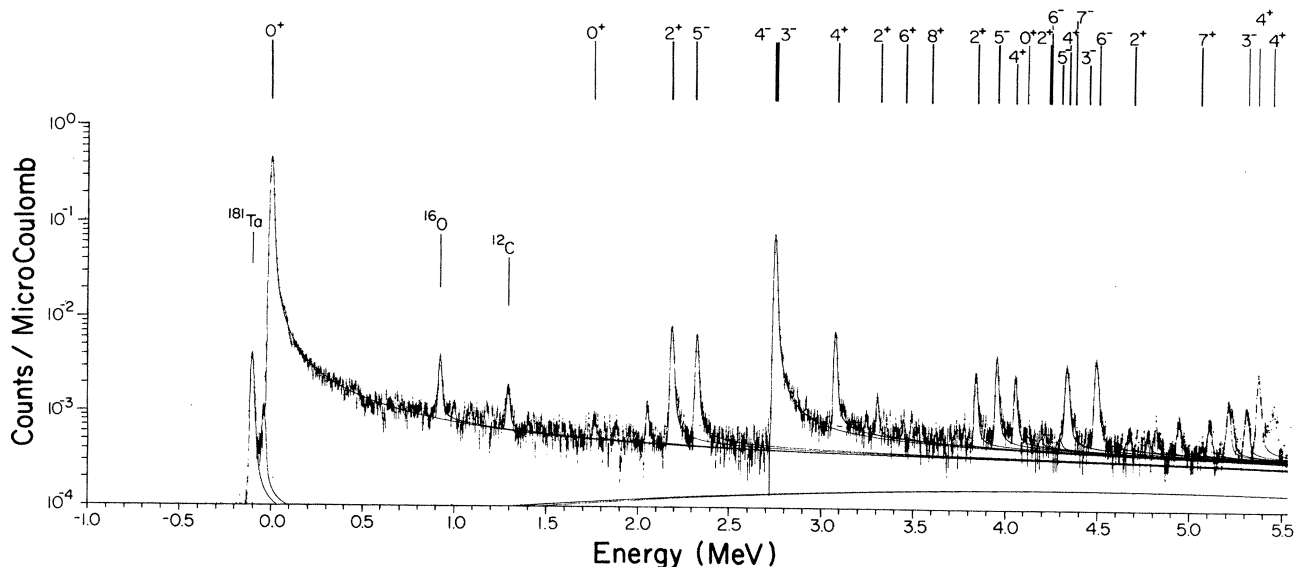

FIG. 2. Spectrum of scattered electrons from ^{90}Zr measured with 150 MeV incident electron energy at 91° scattering angle.

$$q = 2(E_i E_f)^{1/2} \sin\frac{\theta}{2} \ , \tag{4}$$

where θ is the scattering angle and E_f the final electron energy. The form factors are given as Fourier-Bessel transforms of the nuclear transition charge and current densities

$$F_\lambda^C(q) = \frac{\hat{J}_f}{\hat{J}_i} \int_0^\infty \rho_\lambda(r) j_\lambda(qr) r^2 dr \ ,$$

$$F_\lambda^E(q) = - \left[\frac{\lambda-1}{\lambda} \right]^{1/2} \frac{\omega}{qc} F^C(q) - \frac{\hat{\lambda}}{\sqrt{\lambda}} \frac{\hat{J}_f}{\hat{J}_i}$$

$$\times \int_0^\infty J_{\lambda,\lambda+1}(r) j_{\lambda+1}(qr) r^2 dr \ , \tag{5}$$

$$F_\lambda^M(q) = \frac{\hat{J}_f}{\hat{J}_i} \int_0^\infty J_{\lambda,\lambda}(r) j_\lambda(qr) r^2 dr \ ,$$

$$\hat{J} = (2J+1)^{1/2} \ .$$

In this form of F_λ^E, use of the continuity equation has been made to eliminate $J_{\lambda,\lambda-1}(r)$.[16]

All calculations in this data analysis were done in DWBA. In DWBA the simple relation between $d\sigma/d\Omega$ and $\rho(r)$ and $J(r)$ is lost. Still, $d\sigma/d\Omega$ depends on $\rho(r)$ and $J(r)$ and these functions can be reconstructed from the data.[17] Presenting the transition charge or current densities in coordinate space as experimental results is a way to present the results of the experiment in a form where the influence of the distortion of the electron waves has been eliminated. Therefore, the densities lend themselves more for comparison with theoretical predictions than the measured cross sections.

Almost all the transitions discussed in this paper are consistent with assumption of negligible contribution from the current $J_{\lambda,\lambda+1}$. In these cases the extraction of the transition charge density becomes particularly simple since only one density needs to be determined. For those cases it is possible to present the data as recalculated data defined as

$$\frac{d\sigma}{d\Omega}(E_{\max}, q_{\text{eff}})_R = \left[\frac{d\sigma}{d\Omega}(E, q_{\text{eff}}) \right]_{\exp} \left[\frac{d\sigma}{d\Omega}(E_{\max}, q_{\text{eff}}) \Big/ \frac{d\sigma}{d\Omega}(E, q_{\text{eff}}) \right]_{\text{DWBA}} \ . \tag{6}$$

The use of the effective momentum transfer

$$q_{\text{eff}} = q \left[1 + \frac{4Z\alpha\hbar c}{3A^{1/3}E_i} \right] \tag{7}$$

for experimental data corrects to lowest order for the Coulomb attraction between the electron and the nucleus.

For a few levels, a small transverse form factor was observed in our measurement. For those levels, the backward data were fitted separately to determine the size of the transverse form factor using a suitable particle-hole model and keeping the transition charge fixed to the form fitted to the forward scattering data. The data shown for these levels are those forward scattering data obtained after the subtraction of the small transverse form factor as calculated in DWBA, again in the recalculated form.

The high Fourier components in the density were taken into account assuming an exponential upper limit for the form factor above $q_{\max}$ and constraining the tail of the density to an analytic shape $r^{\lambda-1}\exp(-\alpha r)$. This method can be assumed to give a realistic error band for the densities since the data extend to about twice the Fermi momentum where the form factors start to drop rapidly.[16]

IV. RESULTS

A. The proton $(1g_{9/2})^2$ multiplet

The states built from the $\pi(1g_{9/2})^2$ configuration form a multiplet of states with spin and parity 0^+ (1.761 MeV), 2^+ (2.186 MeV), 4^+ (3.076 MeV), 6^+ (3.456 MeV), and 8^+ (3.589 MeV). The 0^+ state contains a strong admixture of

the $(2p_{1/2})^2$ configuration. These states can be excited directly from the nuclear ground state through the strong $(g_{9/2})_0^2$ admixture in the ground state. The excitation proceeds then through the recoupling of the $g_{9/2}$ protons, a process for which the current $J_{\lambda,\lambda+1}(r)$ is absent.[16] The transition charge density $\rho_\lambda(r)$, except for some possible polarization charge, represents the radial density of the $1g_{9/2}$ proton orbit. (This is further discussed in Sec. VI.)

It has been shown for ^{208}Pb (Ref. 4) that for high multipolarities the polarization charges are rather small, therefore we expect that the strength of the $E8$ transition reflects rather well the $g_{9/2}$ occupation probability in the ground state and that the shape of the measured form factor may allow one to determine the radial shape of this $g_{9/2}$ orbit. The argument for this is that, except for the $(1g_{7/2}, 1g_{9/2}^{-1})$ component, which is very similar in shape, there are no other possible $0\hbar\omega$ proton transitions that can couple to 8^+ and thus contribute to this state. $2\hbar\omega$ transitions are, however, far removed in energy and with the weak residual interaction at high momentum transfer, the mixing is supposed to be negligible. This is, however, a quantitative question that will be discussed further in Sec. V. Figure 3 shows the data for this 8^+ state parametrized as a $(g_{9/2})^2$ configuration and recalculated to constant incident energy. The fact that the forward as well as the backward scattering data can be described well, assuming the absence of $J_{\lambda,\lambda+1}(r)$, seems to confirm this assumption.

The spectroscopic amplitude for the $g_{9/2} \rightarrow g_{9/2}$ transition of 0.41 for the 8^+ level is in excellent agreement with the prediction of the pairing calculation by Akkermans[26] of 0.44. Since it is mainly determined by the occupation probability of the $g_{9/2}$ orbit, it confirms that the occupa-
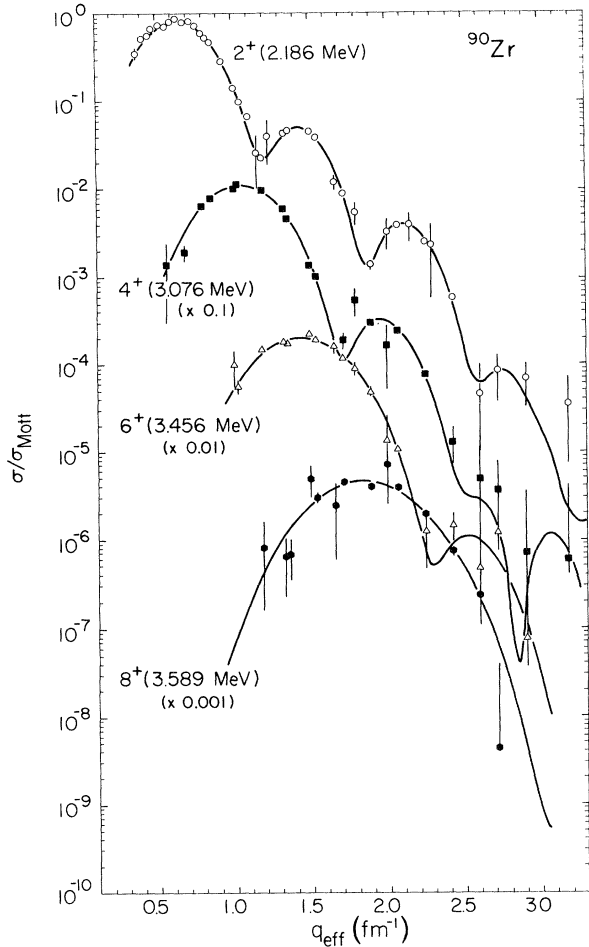
FIG. 3. Cross sections of the 2^+ (2.186 MeV), 4^+ (3.076 MeV), 6^+ (3.456 MeV), and 8^+ (3.589 MeV) state recalculated to incident energy 368 MeV and plotted against q_{eff}. The data are shown together with the best fits. The 4^+, 6^+, and 8^+ data have been scaled down by factors of 0.1, 0.01, and 0.001, respectively.

level but indicates some possible core polarization contribution in the 6^+ level and/or ground state correlations that differ slightly from pairing correlations.

The 4^+ and the 2^+ states have been fitted using the Fourier-Bessel analysis (FBA) as described in Ref. 16. For the 2^+ level we have included in our fit the data from Singhal et al.,[18] from Bellicard as published by Singhal,[19] and from Phan et al.[20] These data were renormalized with respect to the elastic cross section in the same way our data were treated. We also included the $B(E2)$ measurement from photon scattering by Metzger.[21] There is no obvious discrepancy in any of the data as indicated by the fit (see Fig. 3). Again, no contributions from transverse scattering were observed.

Figure 4 shows the best fit transition charge densities with the resulting errors. The error bands for the 6^+ and 8^+ transitions are considerably smaller than for the 2^+ and 4^+ states since the fit was much more restrictive. As can be seen from Fig. 4, all these densities are surface peaked as expected for a (dominant) $1g_{9/2} \rightarrow 1g_{9/2}$ transition. The transition charge density of the 2^+ transition does show some structure in the interior indicating that this transition is no longer a pure $1g_{9/2} \rightarrow 1g_{9/2}$ transition. This result is expected since with the depletion of the $2p_{1/2}$ orbit in the ground state, the $0\hbar\omega$ transitions from $2p_{3/2}$ and from $1f_{5/2}$ to $2p_{1/2}$ are allowed transitions as well and can mix into the lowest 2^+ state.

B. The neutron $(2d_{5/2}, 1g_{9/2}^{-1})$ configuration

The states dominated by the neutron $(2d_{5/2}, 1g_{9/2}^{-1})$ component have been identified through pickup reactions from ^{91}Zr.[3] These experiments show the $2^+, 3^+, \ldots, 7^+$ levels to be at 4.220, 4.578, 4.320, 4.443, 4.528, and 5.050 MeV, respectively. The pure single particle densities indicate that the even spin states show negligible contributions

tion probability $v^2 = 0.15$ of the calculation is in good agreement with our conclusions derived from the comparison of $E5$ transitions in ^{89}Y and ^{90}Zr.[1] The present conclusion may be modified slightly through the presence of core polarization or by the fact that other effects than pairing may contribute to the ground state correlations.

For the 6^+ level we can no longer assume a pure $(g_{9/2})^2$ configuration since $0\hbar\omega$ proton transitions with other shapes are possible. For that reason we describe the data assuming a dominant $1g_{9/2} \rightarrow 1g_{9/2}$ transition with a small admixture of the proton transition from $1g_{9/2} \rightarrow 2d_{5/2}$, the amplitudes of which are determined from a fit to the data. In this fit, the radii of the $\pi 1g_{9/2}$ and the $\pi 2d_{5/2}$ orbits were kept fixed at the value for the $g_{9/2}$ orbit from the 8^+ state. This fit is again shown in the form of recalculated data in Fig. 3.

The fitted amplitudes for the 6^+ transitions give 0.46 for the $\pi 1g_{9/2} \rightarrow 1g_{9/2}$ transition and 0.07 for the $\pi 1g_{9/2} \rightarrow 2d_{5/2}$ transition. The $g_{9/2} \rightarrow g_{9/2}$ amplitude is in close agreement with the results obtained for the 8^+
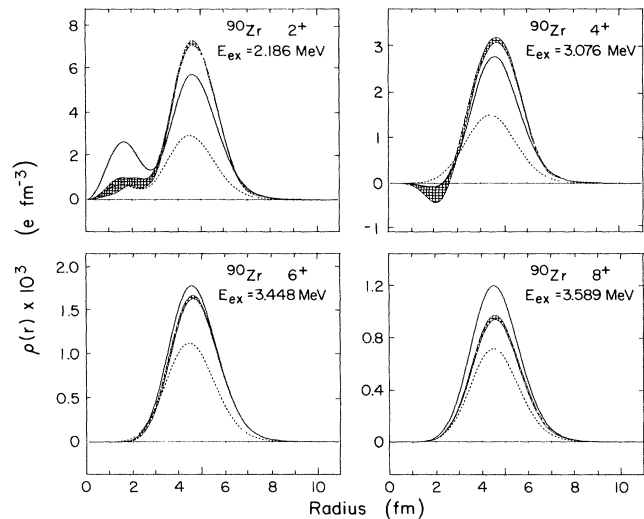

FIG. 4. Transition charge densities for the 2^+, 4^+, 6^+, and 8^+ levels with the dominant configuration $\pi(1g_{9/2})^2$.

in the (ee') cross sections from this neutron configuration. For that reason, electron scattering will see only the induced charge from these transitions.

Of these levels, only the 4^+ state is fully resolved and found at an energy of 4.334 ± 0.002 MeV. The cross sections are small. For that reason this level could be measured only over a limited region in momentum transfer as shown in Fig. 5. We see in our data a strong longitudinal form factor which we fitted using the proton $(2p_{3/2},1f_{5/2}^{-1})$ transition and the $(1g_{9/2},1g_{9/2}^{-1})$ transitions to simulate the core polarization. The configuration with the next higher energy is the $(2d_{5/2},1g_{9/2}^{-1})$ component which is very similar in shape to the $(2p_{3/2},1f_{5/2}^{-1})$ component, and thus is indistinguishable in the fit. Since this exhausts the full variety of shapes within the $0\hbar\omega$ basis, we believe that we can get a good description of the density in spite of the limitation to the two proton components.

The complex at 4.23 MeV appears clearly as an unresolved multiplet. The pickup reactions of Ball and Fulmer[3] show a 2^+ level at this energy, and the (pp') data of van der Bijl *et al.*[15] show at least one additional level. Our data at large momentum transfer indicate a large transverse form factor certainly inconsistent with a 2^+ assignment. This transverse form factor is due to a 6^- state of the dominant proton configuration $(g_{9/2},f_{5/2}^{-1})$. The

structure of this 6^- level will be discussed in a different paper. At low momentum transfer the backward scattering data show very large cross sections that are at too small momentum transfer to originate from the 6^- level. We were unable to account for this strength as transverse electric $E2$ within the basis of the low lying $E2$ transitions. In addition, a careful energy calibration relative to the 5^- level assumed to be at 3.961 MeV or the 2^+ level at 3.843 MeV shows the peak to be at 4.223 ± 0.002 MeV in those spectra where the 2^+ cross section is dominant. The backward measurements at low momentum transfer, however, show the peak at 4.228 ± 0.002 MeV, whereas at high momentum transfer the peak is centered at 4.231 ± 0.002 MeV. This indicates that this complex consists of at least three unresolved levels. These we interpret as 2^+ (4.223 MeV), 4^- (4.228 MeV), and 6^- (4.231 MeV). This 6^- level corresponds to the $(6,7)^-$ level observed in the β decay of ^{90}Nb at 4.2324 MeV.[14]

The fit to the 2^+ level was done to the forward scattering data after subtraction of the backgrounds of the 6^- and 4^- levels. These corrected data together with the fit are shown in Fig. 6. In the fit, the amplitudes for three proton transitions $(1g_{9/2},1g_{9/2}^{-1})$, $(2p_{1/2},2p_{3/2}^{-1})$, and $(2p_{1/2},1f_{5/2}^{-1})$ were adjusted. Again, these shapes exhaust the variety of shapes within the shell model basis. Even
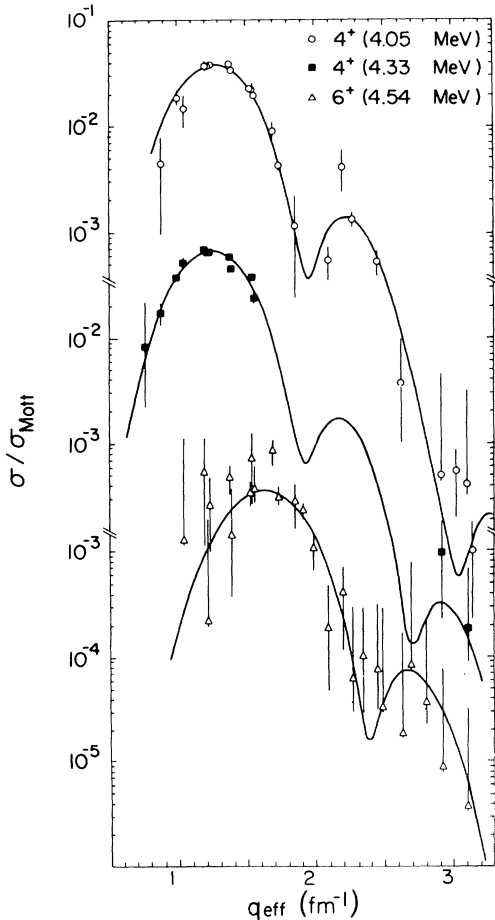

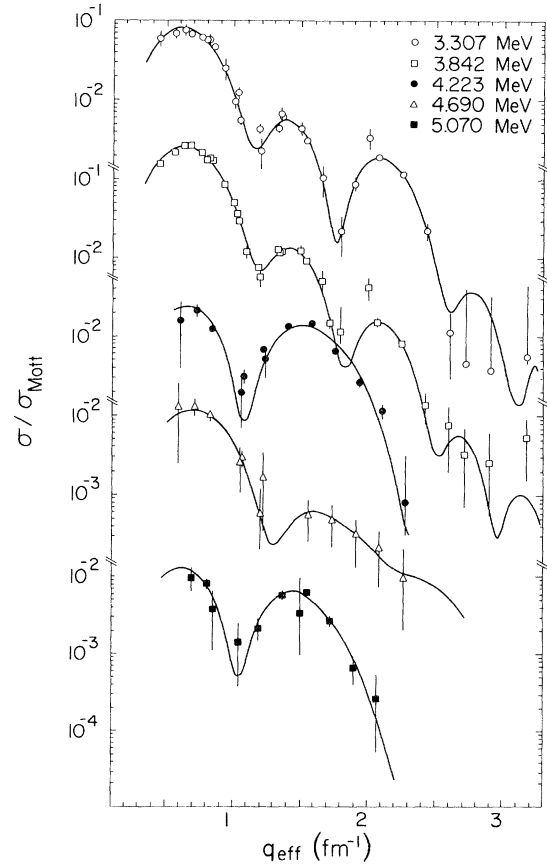FIG. 5. Cross sections for the 4^+ levels at 4.050 and 4.33 MeV, and the 6^+ level at 4.54 MeV.

FIG. 6. Cross sections for the 2^+ levels at 3.307, 3.842, 4.223, 4.690, and 5.070 MeV.

though the fitted values of these amplitudes will have lit-
tle meaning, the resulting transition charge density will be
a fair representation of reality.

The peak at 4.542 MeV is also a doublet. The pickup
experiment shows a 6^+ level of the neutron configuration
at this energy. Our data show a strong transverse form
factor that can only be explained by an unresolved 6^- lev-
el with the dominant proton configuration $(1g_{9/2}, 2p_{3/2}^{-1})$.
Since within the shell model basis there are only two pos-
sible proton configurations for a 6^- state, it is possible to
fit this doublet in spite of the limited information avail-
able. A calibration from those spectra giving the largest
contribution to this 6^+ level shows the excitation energy
at 4.548 ± 0.004 MeV. Again, the data corrected for the
6^- contributions, are shown in Fig. 5 together with the fit.

The odd spin states due to the $(2d_{5/2}, 1g_{9/2}^{-1})$ neutron
configuration should show substantial strength. The most
dominant transition should be the $M7$ transition. We ob-
serve a strong transition with purely transverse nature to a
state at 5.061 MeV. At small momentum transfer, the
forward-angle measurements indicate some longitudinal
form factor which is an indication for an unresolved
natural-parity level. Recent high resolution (p,p') experi-
ments[15] have shown, in addition to the 7^+ level at 5.060
MeV, a level at 5.089 that could possibly be interpreted as
a 1^- level. Our data seem to favor a 2^+ assignment and
we have fitted our data as a sum of a 2^+ and a 7^+ cross
section. The 2^+ data corrected for the background from
the $M7$ and the fit are shown together with the other two
levels in Fig. 6. Because of the dominance of the 7^+ form
factor at larger momentum transfer, this 2^+ level is deter-
mined only over a rather limited region. Nevertheless, the
diffraction minimum is quite well defined. The shape of
the form factor agrees with that of the 4.22 MeV state,
and thus favors the 2^+ assignment over the 1^- assign-
ment. The form factor of the 7^+ level is well defined, in
particular, in backward direction. It allows us to deter-
mine the quenching as well as the radial shapes involved.

Figure 7 shows the data for this 7^+ level and the fit
yielding a neutron $(2d_{5/2}, 1g_{9/2}^{-1})$ configuration of ampli-
tude 0.68 with an admixture of -0.126 from the neutron
$(1g_{7/2}, 1g_{9/2}^{-1})$ component. Calculations from Ref. 26 indi-
cated this configuration to be the largest admixture, how-
ever, with an amplitude much smaller than the fitted
value. The fitted spectroscopic amplitude for the dom-
inant $(2d_{5/2}, 1g_{7/2}^{-1})$ configuration is only little less than
values of 0.707 found for the quenching in the $M14$ and
$M12$ high spin transitions observed in ^{208}Pb.[22] We have
also performed a "model independent" reconstruction of
the current density $J_{\lambda,\lambda}$ using the FBA. The resulting
transition current is shown in Fig. 8.

The data of the 4.46 MeV state, which is supposed to be
the 5^+ state, show much smaller cross sections. For that
reason their relative uncertainties are considerably larger,
and one cannot draw very strong conclusions from these
results. Our data are consistent with the 5^+ assignment
and allow an estimate of the total strength which is in
agreement with the quenching observed for the 7^+ level.

Recently, Fujiwara et al.[23] and van der Bijl et al.[15] have
measured this multiplet in (p,p'). In a microscopic
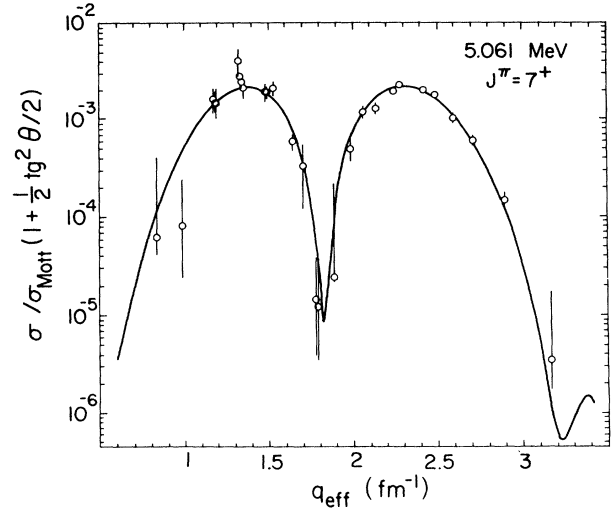analysis, they observe much better agreement with the

FIG. 7. Cross sections for the 7^+ level at 5.06 MeV. The
solid line indicates the best fit to the data.

unnatural-parity states than with the natural-parity states.
From our results, we can see reasons for that situation:
Most importantly, the 2^+ and 6^+ members have substan-
tial contributions from the unresolved two 6^- levels, and
more generally, as is also mentioned by the authors, the
natural-parity states in comparison seem to have much
more configuration mixing than the unnatural-parity
states.

C. Sr-core excitations

Several additional $E2$ excitations have been observed.
The most dominant ones are at 3.307 and 3.843 MeV.
These levels have been fitted including the data of Singhal
et al.[18] and the $B(E2)$ values measured by Metzger.[21]
The FBA has been used to reconstruct the densities in
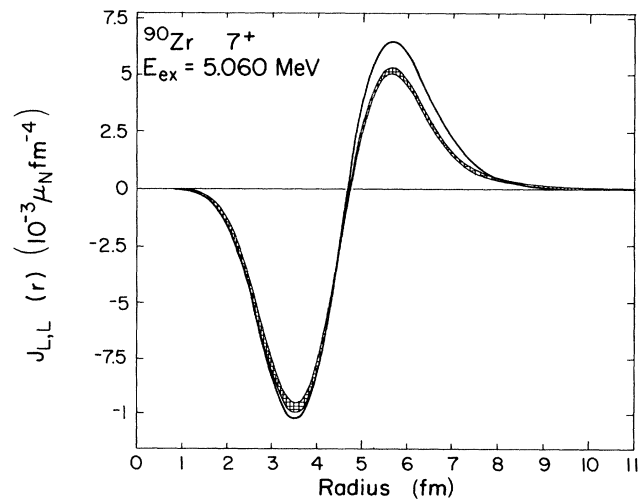coordinate space. The 3.307 MeV level is the only level

FIG. 8. Transition current density for the $M7$ transition to
the 5.06 MeV level. The solid line shows the BP prediction of
Ref. 26.

that showed a substantial transverse form factor. This transverse form factor is expected to arise from the proton $(2p_{1/2}, 1f_{5/2}^{-1})$ and the $(2p_{1/2}, 2p_{3/2}^{-1})$ transitions.[2] We fitted the backward scattering data using a current due to these two components. Figure 6 shows the cross sections measured for these 2^+ levels after subtraction of the transverse contribution. Figure 6 also shows the data of the level at 4.223 MeV discussed above and the levels at 4.690 and 5.070 MeV.

As shown in Fig. 6, the data of the levels of 4.223, 4.690, and 5.070 MeV have rather large uncertainties. This is due either to other unresolved levels, or generally, to the smallness of the cross sections. In these cases, the levels were fitted in a more restricted way as described above for the 4.223 MeV state.

One additional 4^+ state has been observed at the energy of 4.050 MeV. We have fitted the measured cross sections using the FBA to reconstruct the transition charge density. The result is shown in Fig. 9.
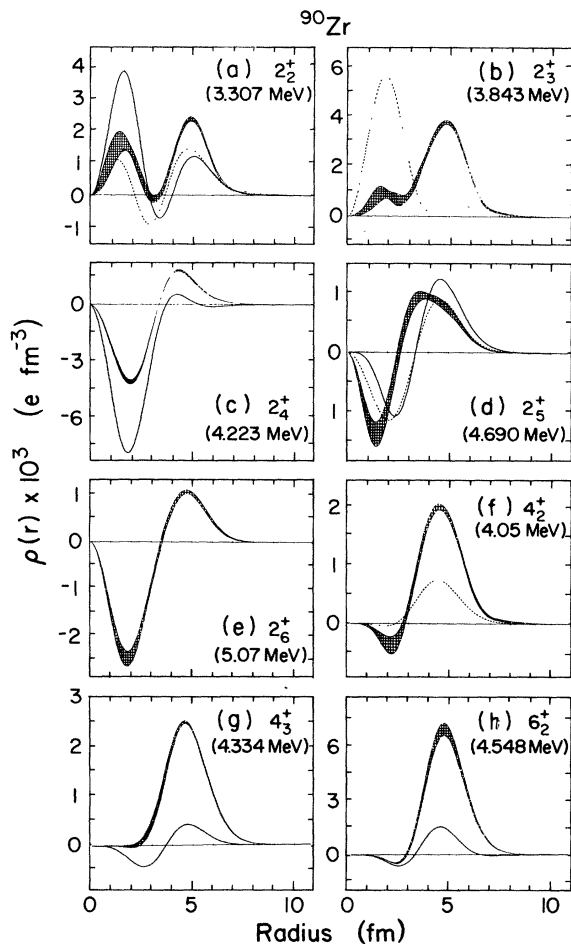
^{90}Zr

FIG. 9. Transition charge densities for the positive parity transitions to the 3.307 MeV (a); 3.842 MeV (b); 4.223 MeV (c); 4.690 MeV (d); 5.070 MeV (e); 4.050 MeV (f); 4.332 MeV (g); and 4.545 MeV (h). The solid line shows the BP predictions of (Ref. 26), the broken lines give the shell model prediction of (Ref. 25).

All the positive-parity proton configurations can be excited only from the ground state component in which at least one pair of protons is in the $g_{9/2}$ shell. In this configuration the remaining nucleons form a ^{88}Sr core which need not necessarily be in its ground state. Thus, in addition to the states of spins 0^+, 2^+, 4^+, 6^+, and 8^+ that correspond to the $(g_{9/2})_J^2$ configuration coupled to the Sr core in its 0^+ state, one should find the equivalent states with the core in any of its excited states. Most prominent are those where the $(g_{9/2})_J^2$ is in the $J^\pi = 0^+$ form and the core is excited to the equivalent states observed in ^{88}Sr. The 3.307 MeV 2^+ state must be interpreted as such a state that corresponds to the lowest 2^+ core excitation. This conclusion follows from energy considerations, since the energy of the second 0^+ state in ^{90}Zr and the energy of the first 2^+ Sr level add up to approximately the observed excitation energy and from the striking similarity of the transition charge density observed for this state (as shown in Fig. 9) and of the one observed in ^{88}Sr.[2] The second 2^+ core excitation in ^{88}Sr is 1.4 MeV above the first one and thus should be found in ^{90}Zr in the vicinity of 4.7 MeV. Indeed, the 4.69 MeV 2^+ state shows a transition charge density (Fig. 9) that in structure is very similar to the transition charge density for the second 2^+ excitation in ^{88}Sr. The pp' experiment of Ref. 15 shows two 2^+ levels at energies 4.69 and 4.71 MeV. In most of our runs, the two levels would not be separated. The two high resolution spectra show, however, that most of the strength comes from the 4.69 MeV state. Since the densities are very similar in shape, we conclude that the strength of the second 2^+ ^{88}Sr core excitation seems to be fractionated between all three observed 2^+ states at 4.232, 4.690, and 5.070 MeV.

By constructing such basis states, one would expect a triplet of states of spins 0^+, 2^+, and 4^+, from coupling the 2^+ core with the $(g_{9/2})_{2+}^2$ around 4.0 MeV. So, we conclude that the second 4^+ state found at 4.05 MeV has as its dominant structure the configuration $[(1g_{9/2})_{2+}^2 \otimes \mathrm{core}_{2+}]_{4+}$. The closeness in energy also indicates the fairly pure nature of this configuration. This state is in energy and structure quite well reproduced by the shell model calculations, but it is outside of the basis for the one broken pair (BP) calculations[26] since such a configuration corresponds to a four-quasiparticle state. Because of this dominant four-quasiparticle nature, the excitation of this state is of particular interest since it may either show the need for such a four-quasiparticle configuration in the nuclear ground state, or it could indicate a strong coupling between two- and four-quasiparticle excitations.

Similarly, we interpret the 3.842 MeV 2^+ state as the corresponding 2^+ state of this multiplet. The 0^+ state at 4.12 MeV has been observed with strong interacting probes.[15] We have not been able to see this level in our data. This is expected since an estimate shows that the cross sections should be below our level of sensitivity.

V. COMPARISON TO NUCLEAR MODEL CALCULATIONS

A realistic calculation of the transitions and their densities causes considerable problems. While random-phase

approximation (RPA) calculations have the main space of ph transitions available and thus could calculate the correct strength, they lack the multiparticle multihole aspect that for the interpretation of the positive parity states in ^{90}Zr is essential. This is quite evident as in such calculations the first 2^+ state appears at 5.36 MeV (Ref. 24) and is dominated by the neutron configuration $(2d_{5/2}, 1g_{9/2}^{-1})$. In the experiment, the neutron dominated 2^+ state is found at 4.20 MeV and is also not the lowest 2^+ state. This is an obvious consequence of the pairing aspect that RPA is unable to describe.

On the other hand, theories that describe the multiparticle multihole character properly, such as the shell model, lack the large enough ph space to predict realistic transition strengths even though the energies of the levels are quite well reproduced. Such calculations have been carried out by Dubach and Haxton.[25] Since the shell model basis has only a small fraction of the total ph basis, the densities calculated are usually much too small.

A different approach is the broken pair approximation used by Akkermans and Allaart.[26] In these calculations the multiparticle multihole aspect is included through a pairing calculation while the one-body densities are increased through a Tamm-Dancoff approximation (TDA) calculation which couples the ph transitions to the quasiparticle excitations. In these calculations the ph basis is still too small so that the calculated densities do not carry enough strength.

In all these calculations the radial shapes of the single particle orbits are not specified. To present definite predictions, we have generated a set of single particle wave functions via Hartree-Fock calculations using the DME interaction of Negele and Vautherin.[27] With the partial occupations as calculated in the shell model, the ground state charge distribution is quite well reproduced as shown in Fig. 1. For that reason, we feel that the use of these single particle wave functions is quite reasonable. The main difference appears in the tail of the density, a problem that shows up similarly in the transition densities predicted with these wave functions.

In Figs. 4 and 9 we compare the experimental results for ρ_{tr} with predictions for the two models: (a) shell model, (b) broken pair calculation. In this comparison, we find that the shell model underpredicts the densities, in particular, for the low multipolarities. This must be viewed as a result that for high multipolarities core polarization plays a minor role.

While BP calculations give a generally improved picture, they underpredict the densities for low multipolarities owing to the still insufficient size of the ph basis while for the high spin states too much strength is predicted. The fact that the density for the 8^+ state is even overpredicted seems to point not only to the limited configuration space but also to the improper q dependence of the residual interaction. The various multipolarities sample the interaction that couples the core excitations to the quasiparticle transitions in the region of the first dominant maximum of their respective form factors. Thus, a long-range force could couple considerable strength from core polarization in the low multipolarities, while almost no strength is coupled into the high multipolarities.

It must be pointed out that the BP model does not give a prediction for the 4.05 MeV 4^+ state. Since this state and the 3.842 MeV 2^+ state have strong four-quasiparticle components, these states are not within the basis of these calculations. Since these states carry considerable strength, it is clear that the BP calculations must fail for 2^+ and 4^+ levels above about 4 MeV. Similarly, the shell model calculations of Dubach and Haxton[25] ignore the neutron configurations which appear at about the same energy. Therefore, these calculations can only be expected to describe the low-lying levels.

For these reasons it is not possible to give a complete correspondence between calculated and measured levels above 4 MeV, and we have in Fig. 9 plotted predicted densities with those levels where the predicted shape matches most closely the observed shape.

In Fig. 8 we also show the transition current density for the 7^+ state using the spectroscopic amplitudes from the calculation of Akkermans.[26] Exchange currents were calculated for the main component and cause a 15% reduction almost independent of the radius. Therefore, we have included a 15% quenching in the magnetization current for all components. The comparison emphasizes the need for this quenching. Some further quenching could be caused by additional ground state correlations. Since the neutron components were included only in the TDA, the calculations do not allow for ground state correlations in the closed shell neutron configuration. However, much more striking seems to be the need for a radius dependent quenching, which within current theories would suggest strong core polarization contributions.

In this connection it is interesting to point out that the relativistic treatment of nucleons inside nuclei in field theories leads to magnetic operators that predict a 30% enhancement of the magnetization density in the interior. While this would produce the observed shape of the transition current, it would increase the prediction even further, and thereby even enlarge the misunderstood discrepancy between prediction and experiment.[28]

VI. THE SIZE OF THE $\pi 1g_{9/2}$ ORBIT

As seen from the considerations of the previous section, core polarization in the 8^+ state plays a rather minor role in the transition charge. Even if there were some contributions to the strength from core polarizations, the major contribution would be from the proton component $(1g_{7/2}, 1g_{9/2}^{-1})$, which is very similar in shape to the dominant configuration and thus does not change the shape in any significant form. For example, in the calculation of Akkermans,[26] core polarization enhances this 8^+ density by 10%. The core polarization changes the radius by 0.1%. The comparison with the experiment suggests that there is considerably less core polarization than predicted in Akkermans's calculation. For that reason, the transition density of the 8^+ level is an ideal measure of the physical extent of the $g_{9/2}$ orbit. This quantity is most properly expressed through the rms radius of the $(1g_{9/2})^2$ point density.

In order to determine this radius one has to convert the transition charge density to the 8^+ level into a point proton transition density. To correct for the proton size, we

have used the recent fit to the proton form factor by Simon *et al.*[29] This deconvolution with the proton size can be conveniently done in the Fourier-Bessel (FB) expansion. If we assume that the point proton transition density for the 8^+ state is expanded in a FB series within a cutoff radius R_c

$$\rho(r) = \begin{cases} \sum A_n j_\lambda(q_n r) & r < R_c \\ 0 & r > R_c \end{cases},$$

then the convoluted density is given by the following:

$$\rho_\lambda^{\text{fold}}(r) = \begin{cases} \sum A_n F_p(q_n) j(q_n r) & r < R_c \\ 0 & r > R_c \end{cases},$$

where $F_p(q_n)$ is the proton charge form factor at $q = q_n$. The cutoff radius R_c has to be chosen large enough so that the assumption $\rho(R) = 0$ does not constitute an unrealistic constraint.

The dominant contribution to the transition charge distribution can be expressed[15] in terms of the radial part $u_{9/2}(r)$ of the $\pi 1g_{9/2}$ wave function as

$$\rho_\lambda^{\text{tr}}(r) = S_\lambda C_\lambda u_{g_{9/2}}^2(r) ,$$

where

$$C_\lambda = (-)^\lambda \frac{10}{4\pi} \langle \tfrac{9}{2} \tfrac{1}{2} \tfrac{9}{2} - \tfrac{1}{2} | \lambda 0 \rangle$$

and S_λ is the spectroscopic amplitude for the $g_{9/2}$ transition. It turns out that for this transition, the relativistic spin-orbit term which was given in Ref. 17, and for this case simplifies to

$$\rho_\lambda^{\text{tr}} = \left[\frac{\hbar c}{2mc^2} \right]^2 2.29 S_\lambda C_\lambda \left[\lambda(\lambda+1) \frac{u^2}{r^2} \right.$$
$$\left. - 10 \frac{1}{r^2} \frac{d}{dr}(ru^2) \right],$$

gives also a significant contribution. It contributes about 10% to the cross section at the maximum of the form factor and modifies slightly the radial shape.

For this investigation, a cutoff radius of 11 fm was chosen. The fitting to the 8^+ level described in Sec. IV A was done with a $g_{9/2}$ orbit generated in a Woods-Saxon well with a diffuseness parameter $a = 0.7$ fm. The well depth was adjusted to produce a separation energy of 6.05 MeV, while a spin-orbit strength of 7.5 MeV was used. The radius of the well and the spectroscopic amplitude were the two parameters fitted. The value of the rms radius is only minimally affected by the choice of the fixed parameters. To account for the uncertainties in the choice of these parameters we have added to the error of the final rms radius the changes in the extracted values to a change in separation energy of 1 MeV, in the diffuseness parameter of 10% and in the spin-orbit strength of 1 MeV. All these variations change the fitted value of the rms radius by much less than the statistical uncertainty, indicating that the rms radius is really determined by the data.

Including these systematic uncertainties, the extracted value for the rms radius of the $1g_{9/2}$ orbit in the center of mass system of the nucleus is

$$R_{g_{9/2}} = 5.035 \pm 0.045 \text{ fm} .$$

This can be compared to the value obtained from the Hartree-Fock (HF) $1g_{9/2}$ orbit as given by the DME interaction of Negele and Vautherin.[27] These HF wave functions are not given in the center of mass system of the nucleus and thus need a correction for the residual center of mass motion of that calculated nucleus. The procedure for this is not unique which will create some small uncertainty in the size of the correction. Since the size of that correction is of the order $1/A$ and thus is only a 1% correction, we will not be concerned here with the various ambiguities. Instead we have adopted the procedure used for harmonic oscillator functions summarized by Überall.[30] Here the wave function is considered to be a convolution of the center of mass fixed single particle wave function with the residual motion of the nuclear center of mass. The latter is assumed to be of the form which is obtained in the harmonic oscillator approximation.

This deconvolution for the c.m. motion can be carried out conveniently with the FB expansion. Assuming the $1g_{9/2}$ proton density is given by

$$\rho(r) = \begin{cases} \sum B_n j_0 \left[\frac{n\pi r}{R_c} \right] & r < R_c \\ 0 & r > R_c \end{cases},$$

the deconvoluted density is given by

$$\rho^{dc}(r) = \begin{cases} \sum B_n F_{\text{c.m.}} \left[\frac{n\pi}{R_c} \right] j_0 \left[\frac{n\pi r}{R_c} \right] & r < R_c \\ 0 & r < R_c \end{cases},$$

where $F_{\text{c.m.}}(q) = \exp(\tfrac{1}{4} a_0^2 q^2 / A)$ is the nuclear center of mass form factor. The harmonic oscillator parameter was chosen $a_0 = 2.2$ fm. The HF prediction gives $R_{g_{9/2}} = 5.012$ fm. This value is in agreement with the experimental result. However, it might be interpreted as a disagreement if one considers the binding energy of the $g_{9/2}$ orbit. The calculated binding energy for the HF $g_{9/2}$ orbit differs from the experimental value which we take to be the removal energy reduced by the excitation energy of this state. A simulation of this effect with the Woods-Saxon (WS) potential shows that this difference in binding energy reduces the HF value for the rms radius by about 2% and increases the difference to the experimental value to about 3%. However, since this simulation is not a self-consistent treatment, it is unclear what the real effect of the incorrect binding energy is.

Our extracted radius has to be seen in contrast to the extraction of the rms radius for the proton $1g_{9/2}$ orbit from magnetic ground state scattering from ^{93}Nb (Ref. 31) or ^{115}In (Ref. 32). The radius extracted in our experiment is about 4% larger than the radius extracted for ^{93}Nb if one assumes that the radius should increase as $A^{1/3}$.

The agreement of the measured orbit size to the level of 4% has to be viewed as successful considering that quite different quantities have been used for the determination. The origin of the remaining 4% difference is not clear and

TABLE II. Fourier-Bessel expansion coefficients using $R_c = 11$ fm for those densities fitted in the FBA.

N	2.186 2^+	3.307 2^+	3.842 2^+	3.076 4^+	4.050 4^+	5.061 7^+
1	6.684 ± 0.254	2.197 ± 0.211	3.834 ± 0.224	2.068 ± 0.315	1.144 ± 0.267	6.046 ± 1.842
2	14.376 ± 0.768	4.309 ± 0.623	7.983 ± 0.664	5.761 ± 0.852	3.290 ± 0.747	12.735 ± 2.250
3	8.429 ± 0.233	2.042 ± 0.184	4.450 ± 0.202	6.289 ± 0.515	3.806 ± 0.465	5.474 ± 1.115
4	-3.387 ± 0.128	-1.484 ± 0.128	-1.864 ± 0.107	2.405 ± 0.194	1.686 ± 0.198	-16.961 ± 3.081
5	-5.497 ± 0.147	-1.467 ± 0.128	-2.624 ± 0.124	-1.200 ± 0.126	-0.644 ± 0.123	-31.988 ± 5.800
6	-0.034 ± 0.086	0.999 ± 0.102	0.461 ± 0.088	-1.410 ± 0.119	-1.096 ± 0.142	-25.475 ± 4.480
7	2.491 ± 0.082	1.833 ± 0.134	1.507 ± 0.085	-0.230 ± 0.117	-0.433 ± 0.133	-9.627 ± 1.819
8	0.919 ± 0.092	0.651 ± 0.093	0.289 ± 0.104	0.051 ± 0.143	-0.079 ± 0.124	-1.104 ± 0.703
9	-0.291 ± 0.116	-0.214 ± 0.169	0.270 ± 0.126	-0.156 ± 0.150	-0.085 ± 0.097	0.174 ± 0.548
10	-0.179 ± 0.174	-0.059 ± 0.182	0.083 ± 0.171	-0.027 ± 0.120	-0.012 ± 0.075	0.028 ± 0.518
11	-0.159 ± 0.197	0.097 ± 0.132	0.080 ± 0.191	0.099 ± 0.072	0.058 ± 0.045	0.097 ± 0.304
12	-0.143 ± 0.204	-0.005 ± 0.087	-0.116 ± 0.115	0.016 ± 0.079	0.018 ± 0.043	-0.057 ± 0.197
13	0.086 ± 0.146	-0.036 ± 0.061	-0.069 ± 0.107	-0.022 ± 0.064	-0.010 ± 0.041	0.019 ± 0.123
14	0.085 ± 0.109	0.017 ± 0.039	0.001 ± 0.099	0.016 ± 0.027	0.008 ± 0.016	-0.014 ± 0.102
15	-0.030 ± 0.111	0.003 ± 0.028	-0.028 ± 0.045	0.007 ± 0.021	0.006 ± 0.010	0.032 ± 0.077
$B(\lambda)^a$	0.653 $E3$ $\pm3.2\%$	0.784 $E2$ $\pm10\%$	0.224 $E3$ $\pm5.8\%$	0.311 $E6$ $\pm10.8\%$	0.910 $E5$ $\pm16.6\%$	0.107 $E13$ $\pm25.2\%$

$^a B(\lambda) = B(E\lambda)$ in units of $e^2 \text{fm}^{2\lambda}$ or $B(M\lambda)$ in units of $\mu_N^2 \text{fm}^{2\lambda-2}$.

one might speculate that for excited states the orbits are less strongly bound, which would lead to a larger radius in such an orbit.

On the other hand, this discrepancy may point to problems with the current operator. It is known that the single particle expressions for currents violate the continuity equation when they are used in conjunction with single particle wave functions calculated with the inclusion of a spin orbit potential.

A full relativistic treatment as in Ref. 28 that does not violate the continuity equation would shift the currents further into the interior of the nucleus and thus possibly explain the observed discrepancy. Such a shift of the currents into the interior has been observed in many inelastic transitions.

VII. CONCLUSION

The levels discussed in this paper are extremely sensitive to the pairing. The quantitative comparison of our results with several theoretical predictions shows that there are two important elements that must be contained in the theory: the pairing aspect and the core polarization aspect. Theories that contain these two aspects can be ex-

pected to describe the results rather well. The members of the $g_{9/2}^2$ band seem to be a particularly interesting sequence of levels for the study of the q dependence of the spin independent part of the residual interaction.

APPENDIX

The parametrization of the transition charge densities is given as

$$\rho_\lambda(r) = \sum_{n=1}^{15} A_n q_n^{\lambda-1} j_\lambda(q_n^{\lambda-1} r) \quad r \le R_c ,$$

where the $q_n^{\lambda-1} R_c$ are the nodes of $j_{\lambda-1}$. The resulting coefficients A_n for a cutoff radius R_c of 11 fm for those densities fitted in the Fourier-Bessel analysis are given in Table II.

Table II also contains the expansion coefficients for the current in the magnetic $M7$ transition which is of the form

$$J_{\lambda\lambda}(r) = \sum_{n=1}^{15} A_n j_\lambda(q_n^\lambda r) \quad r \le R_c .$$

Again, the $q_n^\lambda R_c$ are the nodes of j_λ.

*Present address: Technische Universität München, D-8046 Garching, Federal Republic of Germany.

[1]O. Schwentker, J. Dawson, S. McCaffrey, J. Robb, J. Heisenberg, J. Lichtenstadt, C. N. Papanicolas, J. Wise, J. S. McCarthy, N. Hintz, and H. P. Blok, Phys. Lett. 112B, 40 (1982).

[2]O. Schwentker, J. Dawson, J. Robb, J. Heisenberg, J. Lichtenstadt, C. N. Papanicolas, J. Wise, J. S. McCarthy, L. T. van

der Bijl, and H. P. Blok, Phys. Rev. Lett. 50, 15 (1983).

[3]J. B. Ball and C. B. Fulmer, Phys. Rev. 172, 1199 (1968).

[4]H. Fann, J. P. Schiffer, and U. Strohbusch, Phys. Lett. 44B, 19 (1973).

[5]J. Lichtenstadt, C. N. Papanicolas, C. P. Sargent, J. Heisenberg, and J. S. McCarthy, Phys. Rev. Lett. 44, 858 (1980).

[6]J. Heisenberg, J. Lichtenstadt, C. N. Papanicolas, and J. S. McCarthy, Phys. Rev. C 25, 2292 (1982).

[7]W. Bertozzi, M. V. Hynes, C. P. Sargent, W. Turchinetz, and C. Williamson, Nucl. Instrum. Methods <u>162</u>, 163 (1979).

[8]L. A. Fajardo, J. R. Ficenec, W. P. Trower, and I. Sick, Phys. Lett. <u>37B</u>, 363 (1971).

[9]H. Rothhaas, Ph.D. thesis, Universität Mainz, 1970 (unpublished).

[10]Phan Xuan Ho, J. Bellicard, A. Bussiere, Ph. Leconte, and M. Priou, Nucl. Phys. <u>A179</u>, 529 (1972).

[11]R. P. Singhal, S. W. Brain, C. S. Curran, W. A. Gillespie, A. Johnston, E. W. Lees, and A. G. Slight, J. Phys. G <u>5</u>, 558 (1975).

[12]G. Fricke *et al.* (private communication).

[13]J. L. Friar and J. W. Negele, *Advances in Nuclear Physics,* edited by M. Baranger and E. Vogt (Plenum, New York, 1975), Vol. 8, p. 219.

[14]D. C. Kocher, Nucl. Data Sheets <u>16</u>, 55 (1975).

[15]L. T. van der Bijl, H. P. Blok, J. F. A. van Hienen, and J. Blok, Nucl. Phys. <u>A393</u>, 173 (1983).

[16]J. Heisenberg and H. P. Blok, Annu. Rev. Nucl. Part. Sci. <u>33</u>, 569 (1983).

[17]J. Heisenberg, *Advances in Nuclear Physics,* edited by M. Baranger and E. Vogt (Plenum, New York, 1981), Vol. 12, p. 61.

[18]R. P. Singhal, S. W. Brain, W. A. Gillespie, A. Johnston, F. W. Lees, and A. G. Slight, Nucl. Phys. <u>A218</u>, 189 (1974).

[19]J. Bellicard, Ph. Leconte, T. H. Curtis, R. A. Eisenstein, D. Madsen, and C. Bockelman, Nucl. Phys. <u>A143</u>, 213 (1970).

[20]Phan Xuan Ho, J. Bellicard, Ph. Leconte, and I. Sick, Nucl. Phys. <u>A210</u>, 189 (1973).

[21]F. R. Metzger, Phys. Rev. C <u>9</u>, 1525 (1974).

[22]J. Lichtenstadt, J. Heisenberg, C. N. Papanicolas, C. P. Sargent, A. N. Courtemanche, and J. S. McCarthy, Phys. Rev. C <u>20</u>, 497 (1979).

[23]M. Fujiwara, Y. Fujita, S. Morinobu, I. Katayama, T. Yamazaki, T. Itahashi, H. Ikegami, and S. I. Hayakawa, Phys. Lett. <u>106B</u>, 51 (1981).

[24]J. Decharge (private communication); D. Gogny, in *Lecture Notes in Physics,* edited by H. Arenhövel and D. Drechsel (Springer, New York, 1979).

[25]J. Dubach and W. Haxton, calculations using Kuo-Brown-matrix elements (private communication).

[26]J. N. L. Akkermans, Ph.D. thesis, Vrije University, Amsterdam, 1981; K. Allaart (unpublished).

[27]J. W. Negele and D. Vautherin, Phys. Rev. C <u>5</u>, 1472 (1972).

[28]B. D. Serot, Phys. Lett. <u>107B</u>, 263 (1981).

[29]G. G. Simon, Ch. Schmitt, F. Borkowski, and V. H. Walther, Nucl. Phys. <u>A333</u>, 381 (1980).

[30]H. Überall, *Electron Scattering from Complex Nuclei* (Academic, New York, 1971).

[31]S. Platchkov, J. B. Bellicard, J. M. Cavedon, B. Frois, D. Goutte, M. Huet, P. Leconte, Phan Xuan Ho, P. K. A. deWitt Huberts, L. Lapikas, and I. Sick, Phys. Rev. C <u>25</u>, 2318 (1982).

[32]L. Lapikas, in *Proceedings of the International Conference on Nuclear Physics with Electromagnetic Interactions,* Mainz, 1979, edited by H. Arenhövel and D. Drechsel (Springer, Berlin, 1979), pp. 41–51.